A Theoretical Approach to Demystify the Role of Copper Salts and O_2 in the Mechanism of C-N Bond Cleavage and Nitrogen Transfer

Boyli Ghosh[a], Ambar Banerjee[b], Lisa Roy[c], Rabindra Nath Manna[a], Rounak Nath[a], Ankan Paul*[a]

[a] Boyli Ghosh, Rabindra Nath Manna, Rounak Nath, Ankan Paul*
School of Chemical Sciences
Indian Association for the Cultivation of Science
2A & 2B, Raja S. C. Mullick Road, Jadavpur,
Kolkata, 700032 India
E-mail: rcap@iacs.res.in

[b] Ambar Banerjee
Department of Physics
Stockholm University
Frescativägen, 114 19 Stockholm,
Sweden

[c] Lisa Roy
Institute of Chemical Technology Mumbai - IOC Odisha Campus Bhubaneswar,
IIT Kharagpur Extension Centre,
Bhubaneswar, 751013 India

Supporting information for this article is given via a link at the end of the document.

Abstract: C≡N bond scission can be a potential avenue for functionalization of chemical bonds. Primarily, rupture of C≡N bonds in organonitriles are accomplished by protonation, reductive cleavage and metathesis techniques to furnish metal nitride moieties suitable to execute nitrogen transfer reactions. We have conducted an extensive computational study, using density functional theory (DFT), to unravel the intricate mechanistic pathways traversed in the copper-promoted C≡N bond cleavage of coordinated cyanide anion under a dioxygen atmosphere, which enables a nitrogen transfer to various aldehydes. Furthermore, detailed electronic structure analysis of the intermediates and the transition states along with the mechanistic corridors using ab initio multireference CASSCF calculations for two different copper promoters, CuCN and $CuBr_2$, revealed that in both cases radical based pathways are operatives, which is in sound agreement with the experimental findings. This is a unique instance of oxygen activation mechanism which is initiated by single electron transfer from the carbon centre of the nitrile moiety; whereas the major driving force of this mechanism is $Cu^{II/I}$ redox cycle operating on the metal centre. Our study revealed that the copper salts act as the “electron pool” in this unique nitrogen transfer reaction forming aryl nitrile from aryl aldehydes.

Introduction

Functionalization of C-C bonds are pervasive in fundamental biological processes, for e.g. metabolism of carbohydrates, in large-scale industrial operations, like oil production from hydrocarbons and degradation of plastics etc..[1-3] Although development of new techniques for formation of C-C bonds or its cleavage, either catalytically or employing high energy intermediates has been studied extensively, creating new methodologies for selective transformation of multiple bonds containing C≡X motifs (where X is C or N), is still underdeveloped.[4-6] This is primarily due to the thermodynamic and kinetic challenges associated with the dissociation of multiple bond linkages (bond dissociation energy of C≡C is 230 kcal/mol and that of C≡N is 223 kcal/mol).

The past few decades have witnessed several ardent efforts to develop transition metal-based catalysis of C≡C bond activation as a promising synthetic tool in synthesis of complex molecules and polymeric systems.[2] Pioneering works from the groups of Chauvin, Grubbs and Schrock in the field of olefin metathesis reactions and unusual C-C bond formation led to the synthesis of highly efficient ruthenium, molybdenum and tungsten catalysts, making several impactful discoveries and benefitting academia and industries equally.[7-15] Application of this class of catalysts for chemical transformations of dienes, enyne and dienyne compounds have made significant advancement in ring-closure, cross and combination metathesis reactions. In recent years, metal-mediated functionalization of C≡N triple bonds in organonitriles has also been explored.[16-17] Primarily, rupture of C≡N bonds is accomplished by the dual protonation of the distal nitrile carbon, reductive cleavage and metathesis techniques to furnish metal nitride (-M≡N) moieties suitable to execute nitrogen transfer reactions.[7-19] For instance, Tanabe *et al.* have demonstrated a molybdenum dinitrogen complex cleaving C≡N triple bonds of various β-ketonitriles which yield (nitride)(nitrile-enolate) complexes.[19] Sun *et al.* developed a C-C metathesis route comprising three organonitrile molecules with one Si-tethered diyne unit to afford a pyrrole derivative, promoted by a low-valent zirconocene species.[9] Kawashima and others synthesized a tri-ruthenium cluster to facilitate C≡N cleavage of benzonitrile to yield a unique μ_3-nitrido-μ_3-allyl complex.[17] However, C≡N triple bond cleavage of a metal-coordinated cyanide anion is extremely challenging, even more difficult than N≡N triple bond cleavage,[4-6] and remains primarily unexplored. It has been suggested that due to the negative charge on the CN^- anion, the π* orbitals are raised in energies, thereby precluding back-donation from metal for a feasible C-N scission.[19]

In fact, binuclear model systems of the type [L_3Mo–CN–MoL_3] are found to undergo dissociation to [L_3Mo–C]$^-$ and [N–MoL_3] at very high activation energies, which possibly explains the dearth in successful experiments leading to cyanide cleavage.[6] In this context, an intriguing breakthrough has been achieved by Wu *et al.* with copper salts which promote the cleavage of a copper coordinated C≡N bond.[20] Unlike previous attempts which employed heavy 4*d* or 5*d* transition metal like molybdenum or tantalum, utilization of an earth-abundant versatile metal like copper is a novel idea. The ability of copper to easily achieve several oxidation states via single electron or two electron redox processes makes them an ideal candidate for several intriguing stoichiometric and catalytic organic transformations taking place by radical or reductive elimination pathways.[21-29] Furthermore, oxidation of copper with the environment friendly oxidant, O_2, allows the metal to achieve different oxidation states quite easily.[30-32] This leads to a promising pathway for synthesis of nitriles from aldehydes, choosing an appropriate cyanide source and the Cu(I)/Cu(II) salt. (Scheme 1).[20]

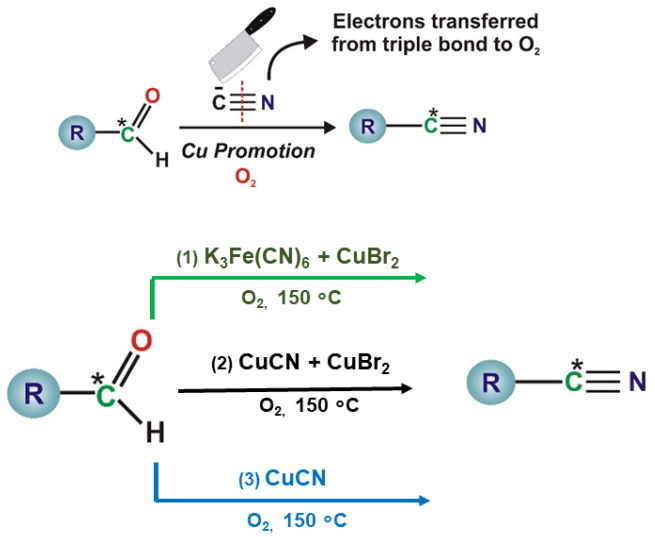

Scheme 1: a) Reaction conditions for copper mediated cyanide cleavage to generate nitrile from aldehyde.

Interestingly, isotope labelling experiments have confirmed the transfer of nitrogen atom attached to the cyanide anion to various aldehydes to form aryl nitrile complexes. Although some theoretical studies have indicated cleavage of a bridging C-N triple bond in a bimetallic system, similar to that observed for N_2 cleavage,[6] elucidation of the mechanism of terminal C≡N bond scission remains uncharted in the literature. Specifically, Wu *et al.* demonstrated C-N cleavage leading to nitrogen transfer to aryl aldehydes in the presence of both $Cu^{I}CN$ and $Cu^{II}Br_2$/ $K_3[Fe(CN)_6]$ combination.[20] This suggests the possible intermediacy of $Cu^{I}CN$ during nitrogenation of R-C(=O)-H (R=aryl) species which needs to be rationalized from a theoretical perspective. Furthermore, these transformations are fascinating because of the involvement of aerial oxygen which plausibly involves a spin-forbidden reaction. O_2 activation involves different spin states on the dioxygen and the activating agent where spin orbit coupling effects are expected to play important roles and warrants an in-depth *ab initio* multi reference treatment to understand the electron transfer pathways. Hence, it is imperative to carry out a detailed theoretical investigation to understand the electron transfer mechanism occurring in these reactions. In this work, we therefore explore the scope of combined density functional theory (DFT) and complete active space self-consistent field (CASSCF) approach to study the mechanism of O_2 activation and the overall reaction leading to C≡N cleavage. We believe these theoretical insights would provide better understanding of the molecular machines and inspire applications with broader substrate scope.

Results and Discussions

You and co-workers in their study (Scheme 1).[20] used both Cu(I) and Cu(II) resources, under two different reaction conditions and obtained the same aryl nitrile product of comparable yield. Among the Cu(II) salts used, $CuBr_2$ afforded a higher yield than that by $CuCl_2$ in the presence of a cyanide source. The Cu(I) salt CuCN gave much higher yield compared to that of CuCl in the absence of any cyanide source. When the copper salt $CuBr_2$ is used as a promoter, potassium ferricyanide, $K_3[Fe(CN)_6]$ or CuCN is required; whereas when CuCN is used it acts both as a copper and a cyanide source. Either of the combinations: (1) $K_3Fe(CN)_6$ + $CuBr_2$ (2) CuCN + $CuBr_2$ and (3) CuCN (only) works fine (Table ST1 for experimental reaction conditions in ESI). This shows that the presence of iron is not imperative, but copper is. In short, a copper salt, and a cyanide ion (CN^-) source and O_2 can facilitate this transformation. You and co-workers in their report have proposed a radical pathway which initiates through a H atom abstraction from the aldehyde.

Notably, the proposed pathway is applicable to the Cu(I)CN based system only. The authors surmise that probably a similar channel operates for the $K_3Fe(CN)_6$ + $CuBr_2$ system through a redox corridor. Nevertheless, as no theoretical validation was presented, multiple possibilities have to be evaluated. Furthermore, one is certainly tempted to enquire, is there is a general mechanism which propels this unique multiple bond cleavage. We focused our efforts on understanding the Cu(II) based systems with cyanide source, primarily on the $K_3Fe(CN)_6$ + $CuBr_2$ system which was reported to be the most efficient promoter. It must be noted that the lone experimental report had convincingly proven that the reaction propagates through radical channels. [20] Furthermore, the authors hypothesize that aerial oxygen first oxidize the Cu(I) center to Cu(II), which acts as a single electron oxidant converting aldehyde to acyl radical species. Subsequently the $Cu^{I}CN$ salt assists the coupling of the acyl radical with the coordinated cyanide to generate another carbon centered radical intermediate. Subsequently the radical species interacts with aerial oxygen to form an isocyanate intermediate, which releases CO_2 to give the desired nitrile compound, suggesting the involvement of isocyanide intermediate during nitrogen transfer process. This oxidation process is predicted to eliminate $Cu^{II}O$ species which has been detected by X-ray photoelectron spectroscopy on analysis of the solid product (Scheme S1 in ES1). Previous experimental and computational studies have showed that the resulting isocyanate species give the cyanated product with the release of carbon dioxide.[55]

Differential Solvation of the Copper Salts

To understand the mechanistic channels, it is paramount to have a clear understanding of the solvation of the active metal species in the solvents. The copper salts CuCN and $CuBr_2$ can interact favorably with the carboxyl group of the DMF solvent. To gain insights on the differential solvation of the copper salts and identify the active solvated species taking part in the chemical reaction both the copper salts were solvated separately in a cubic box of DMF.

Both the systems were minimized with 50000 steps of steepest decent method followed by 1 ns simulation using NVT ensemble at 423K and followed by 100 ns production MD simulations were run using NPT ensemble. The systems were found to maintain an equilibrium temperature and density close to the experimental data throughout the simulations (Figure S1-S3 in ESI). Finally, the equilibrium simulation calculation was carried out for both the systems i.e. which yielded the equilibrated structures with unique arrangements of DMF molecules around CuCN and $CuBr_2$. The final frame of molecular dynamic simulation result had two molecules of DMF solvent in the first sphere of solvation of CuCN (distance between Cu^{I} center and oxygen atom of two DMF molecule is 4.40 Å and 4.48 Å respectively) and one DMF solvent in the first solvation sphere of $CuBr_2$ (distance between Cu^{I} center and oxygen atom of the DMF molecule is 4.50 Å). The solvent molecule arrangement within the first solvation sphere (4 Å) of the copper salts was considered as a guess for carrying out optimization using the DFT methods (Figure 1a-d). One and two molecules of DMF were found to form bonds with copper center of CuCN and $CuBr_2$ respectively.

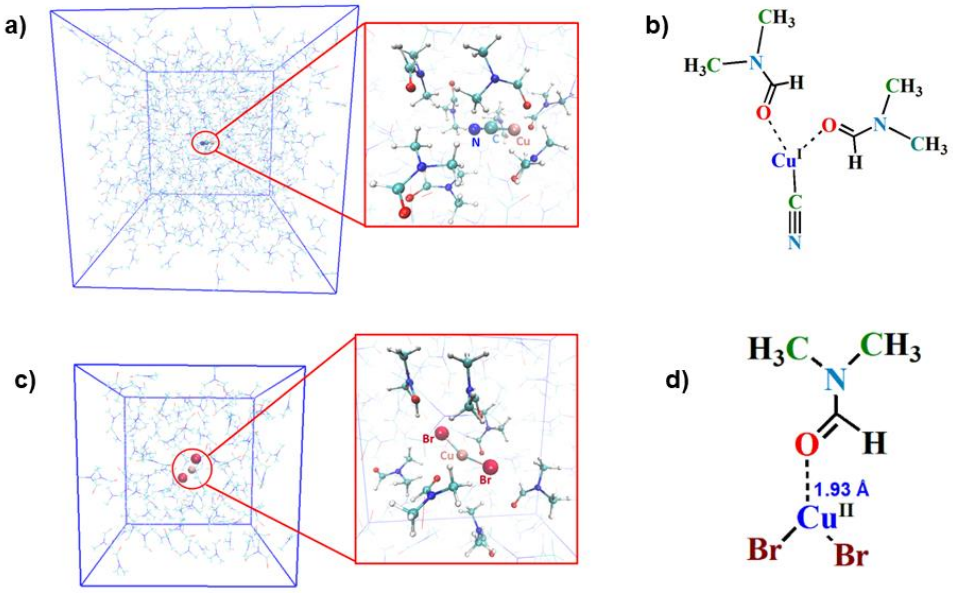

Figure 1: (a) A snapshot of CuCN moiety along with solvent molecules within 4 Å of CuCN inside the DMF box after 100 ns MD simulations. (b) DMF coordinated species with CuCN salt after DFT optimization (**1ª**) (c) A snapshot of $CuBr_2$ moiety along with solvent molecules within 4 Å of CuCN inside the DMF box after 100 ns MD simulations. (d) DMF coordinated species with $CuBr_2$ salt after DFT optimization (**1ᵇ**).

Invariably, in the DFT-optimized structures at B3LYP/B1, two DMF molecules remain coordinated to the Cu^{I} center of CuCN and one DMF molecule remain coordinated to the Cu^{II} center of $CuBr_2$. In the potential energy surface calculation, we considered these DMF coordinated copper salts to be the active substrate.

Nucleophilic Addition of Cyanide Anion and Proton Abstraction Steps

Benzaldehyde was chosen as the model aldehyde substrate.[20] Theoretical calculations predict that the cyanide source $K_3Fe(CN)_6$ can release more than one free cyanide anion in the reaction medium at the reaction temperature of 150°C in the presence of DMF solvent. Subsequent release of the first and the second cyanide anion (CN^-) from one molecule of $K_3[Fe(CN)_6]$) requires 13 kcal/mol and 21 kcal/mol respectively. After the release of CN^- the binding sites are replaced by one and two DMF molecules which provide stabilization to the resulting complex. The Cu-CN bond is covalent in nature and the dissociation energy of CN^- anion from free CuCN is extremely high (52 kcal/mol), however, the solvated copper salt, where CuCN is coordinated to two explicit DMF solvent molecules can release CN^- at a much lower dissociation energy barrier (24 kcal/mol).

MD simulation results predicted that the Cu^{II} center in $CuBr_2$ (d^9 system) remains coordinated to the carboxyl group of one DMF solvent molecule in solution, possibly due to the unpaired spin on the metal center, . We used the $CuBr_2$-DMF adduct, **1ª**, as the starting active compound for calculating the free energy surface of the nitrogen transfer reaction mechanism, assisted by cyanide anion released from $[Fe(CN)_6]^{3-}$ (Figure 2a). The DMF solvent was substituted by the substrate benzaldehyde to form the slightly destabilized (5.1 kcal/mol) intermediate, **2ª.** In intermediate **2ª**, the carbon center of the carbonyl moiety is slightly electropositive in nature and is prone to undergo a nucleophilic attack by the cyanide anion. The cyanide ion coordinates loosely to the carbonyl center in intermediate **3ª** followed by cyanide ion attack on the carbonyl group of benzaldehyde via a transition state, **TS-1ª** (16.5 kcal/mol), forming a stabilized nitrile adduct, **4ª** (-4.3 kcal/mol). Subsequently, a second cyanide anion abstracts the proton attached to the carbonyl carbon via **TS-2ª** overcoming a barrier of 33.6 kcal/mol. This proton abstraction step leads to the formation of a highly stabilized intermediate, $CuBr_2$ coordinated 1-benzoyl cyanide,**5ª** (-0.9 kcal/mol). In the next step the $CuBr_2$ moiety get transferred from the carbonyl oxygen to the nitrogen atom of the coordinated nitrile moiety transition state, **TS-3ª** (8.1 kcal/mol) to form the slightly stabilized intermediate, **6ª** (-3.07 kcal/mol).

In order to understand how the electronic structure governs the outcome of this reaction channel, we have carefully analyzed the electronic structure and the frontier orbital picture evolution during the transformation. In the reactant complex, **2ª**, before oxidative addition of CN^- ion, the carbonyl moiety possesses a C-O π bonding orbital (O 74% C 23%) along with a σ bonding orbital. The carbonyl bond in complex **2ª**, has a double bond character with C-O bond length of 1.23 Å. After the addition of the nitrile moiety, the double bond character of the carbonyl moiety is reduced and the α- electron on the oxygen p-orbital overlaps with the β-electron on Cu-d_{z^2} orbital (O 65% Cu 35%). As a result, the C-O bond elongates to 1.39 Å and the Cu-O bond shrinks to 1.89 Å in complex **4ª**. In contrast, the SOMO (single occupied molecular orbital) is a Cu and Br based orbital (Cu 49 % Br 43 %) in complex **2ª**, which slightly gets delocalized on the oxygen atom in complex 4ª (Cu 53 % Br 16 % O 19 %) (Figure 2a). In the next hydrogen abstraction transition state, **TS-2ª** the oxygen p-orbital overlap increases with the Cu d_{z^2} orbital (O 34% Cu 62 %) and the spin population analysis reveals that an electron is transferred from the carbonyl moiety to the Cu^{II} center in this step.

Hence, on the abstraction of the proton, the carbonyl moiety gets oxidized itself, reducing the Cu^{II} center to Cu^{I} center. In complex **5ª** the oxygen-copper overlapped orbital vanishes and a C-O π orbital is formed. Therefore, in complex **5ª** the C-O bond shrinks to 1.30 Å and O-Cu bond elongates to 2.01 Å, and the SOMO is a carbon, oxygen and nitrogen-based orbital (O 22% C 32% N 14%). On formation of complex **5ª** the orbital overlap between the p-orbital of carbonyl oxygen and d-orbital of Cu is reduced, and a carbonyl π-orbital is generated. This weakening of the bonding interaction between the carbonyl oxygen center and the copper center leads to the transfer of $CuBr_2$ moiety to nitrogen atom of the nitrile moiety via a low barrier transition state **TS-3ª.** (Figure S4 in ESI for detailed FMO pictures and spin population analysis).

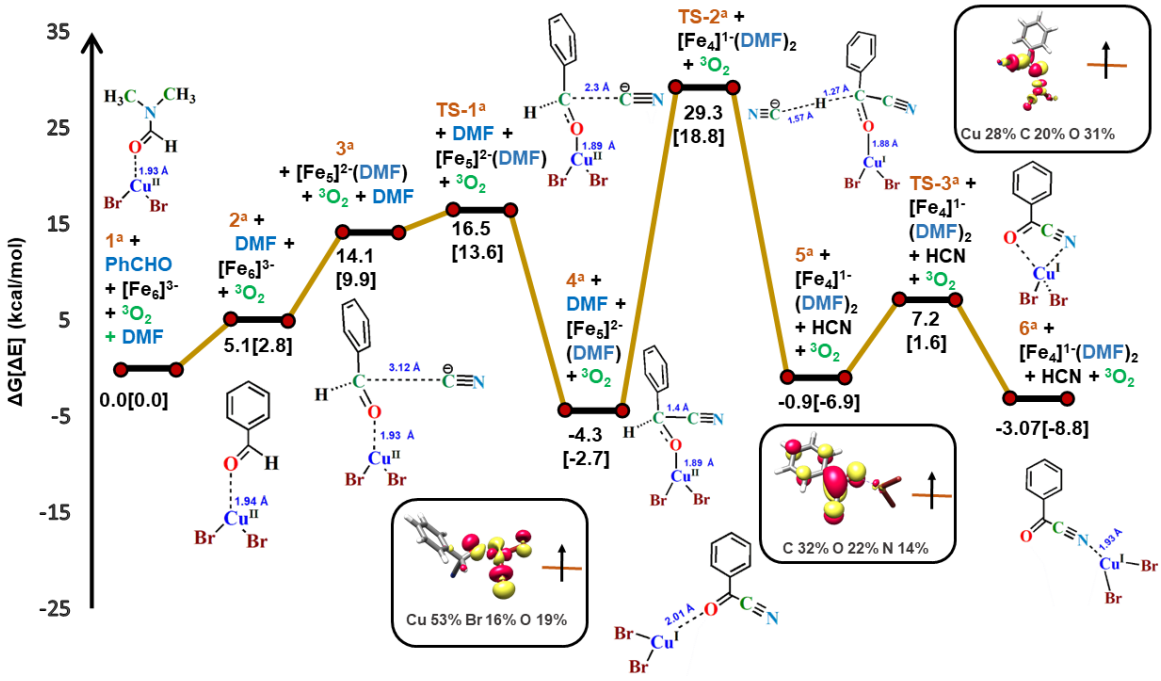

Figure 2a. Computed B3LYP/B1 Gibbs free energy (ΔG) profile for reaction of benzaldehyde with cyanide anion and $CuBr_2$ on the doublet potential energy surface. Singly occupied molecular orbitals for intermediate **4ª**, **TS-2ª** and **5ª** are shown in inset. $[Fe(CN)_6]^{3-} \equiv [Fe_6]^{3-}$, $[Fe(CN)_5]^{2-} \equiv [Fe_5]^{2-}$ and $[Fe(CN)_4]^{1-} \equiv [Fe_4]^{1-}$ representations are used in the figure. Quantities within the square bracket represents total energy change in kcal/mol [ΔE].

Oxygen Activation by $CuBr_2$-1-benzoyl cyanide (6ª)

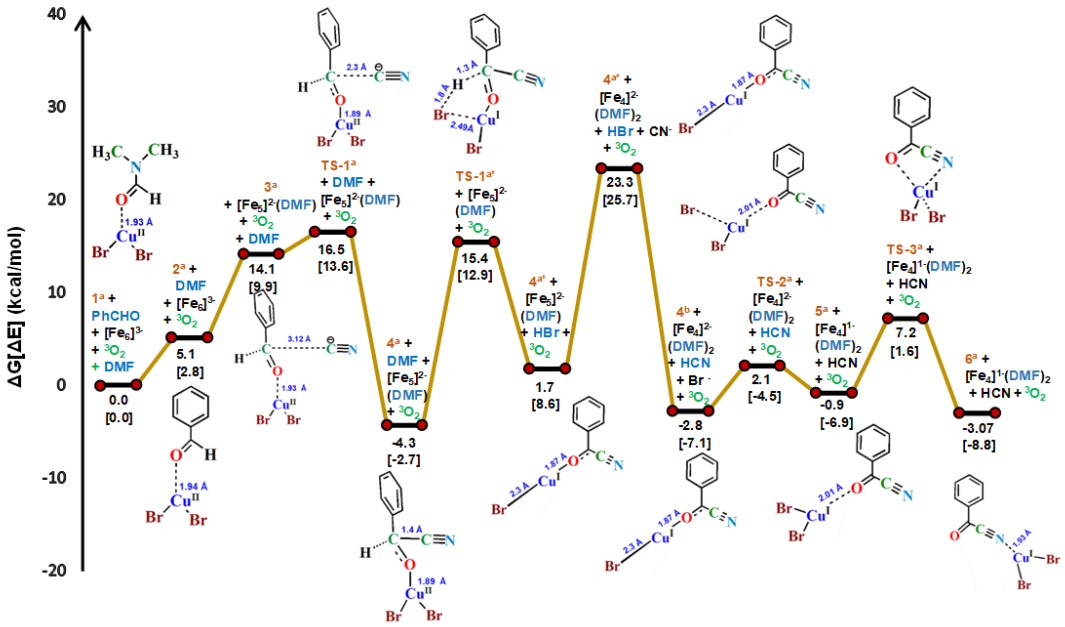

Figure 2b. Alternative Gibbs free energy (ΔG) pathway of proton abstraction and HBr release computed using B3LYP/B1 level of theory.

An alternate mechanistic possibility (Pathway A*) arises if the hydrogen abstraction is done by the bromine ion of $CuBr_2$ (Figure 2b). This bromine ion abstracts the proton via **TS-1^{a*}** having a barrier of 19.7 kcal/mol to releasehydrogen bromide and yields a slightly destabilized (1.7 kcal/mol) intermediate, **3^{a*}**. In the next step, HBr coordinates with a CN^- ion released from the cyanide source, to form more stabilized HCN and Br^- is released in the reaction medium. The RDS is the CN^- ion release from the cyanide source having a barrier of 27.6 kcal/mol. In the next step, the bromide anion attacks the copper center to form $CuBr_2$, and follows the same reaction pathway as Pathway A.

Reaction of complex **6^a** having a doublet ground state with aerial oxygen having triplet ground state will lead to two possibilities quartet and doublet spin state reaction coordinates. We have examined the formation of doublet intermediate **7^a** starting from reactants with doublet intermediate **6^a** and triplet oxygen on quartet surface. The, oxygen bound intermediate **7^a** have a doublet ground state and the intermediate with quartet spin state, **[7^a]^Q** is high lying (29.4 kcal/mol) compared to its ground state. The formation of oxygen coordinated doublet intermediate **7^a**, from doublet intermediate **6^a** and triplet oxygen is spin forbidden in nature (Figure 3). So, a minimum energy crossing point (MECP) has to be located here where the potential energy surfaces of different spins intersect one another. Such MECP can be located proficiently by the gradient based optimization methods and can be efficiently done by a code developed by Harvey *et al*.[33] **MECP 1^a** lies at a barrier height of 6.2 kcal/mol. Soon after the spin crossover, a doublet intermediate, **7^a** (-4.9 kcal/mol) is formed where the oxygen coordinates both with the carbon centre of the nitrile moiety and the Cu centre. Immediately after the formation of intermediate **7^a** the O-O π bond is cleaved forming a σ bond between the carbon centre of nitrile and oxygen end via **TS-4^a** surmounting a barrier of 8.8 kcal/mol. Intermediate **8^a** is found to be 4.6 kcal/mol stabilised with the Cu centre interacting with the other end of oxygen. In the next step O-O σ-bond cleaves via **TS-5^a** overcoming 18.0 kcal/mol to form intermediate **9^a** (-1.3 kcal/mol) bearing a Cu-O single σ-bond and C-O double bond. Immediately after formation **9^a** undergoes a Hofmann rearrangement via low barrier (1.1 kcal/mol) transition state, **TS-6^a** and leads to the formation of the key benzoyl isocyanate product, **7** and di anionic Cu^I-oxyl dibromide, **10^a** ($^{\bullet}$O-Cu^IBr_2)^2 or Cu^{II}-oxide dibromide ($^-$O-$Cu^{II}Br_2$)$^{2-}$ (Figure 3). This isocyanate product gives the copper nitrile product with concomitant release of CO_2.[55]

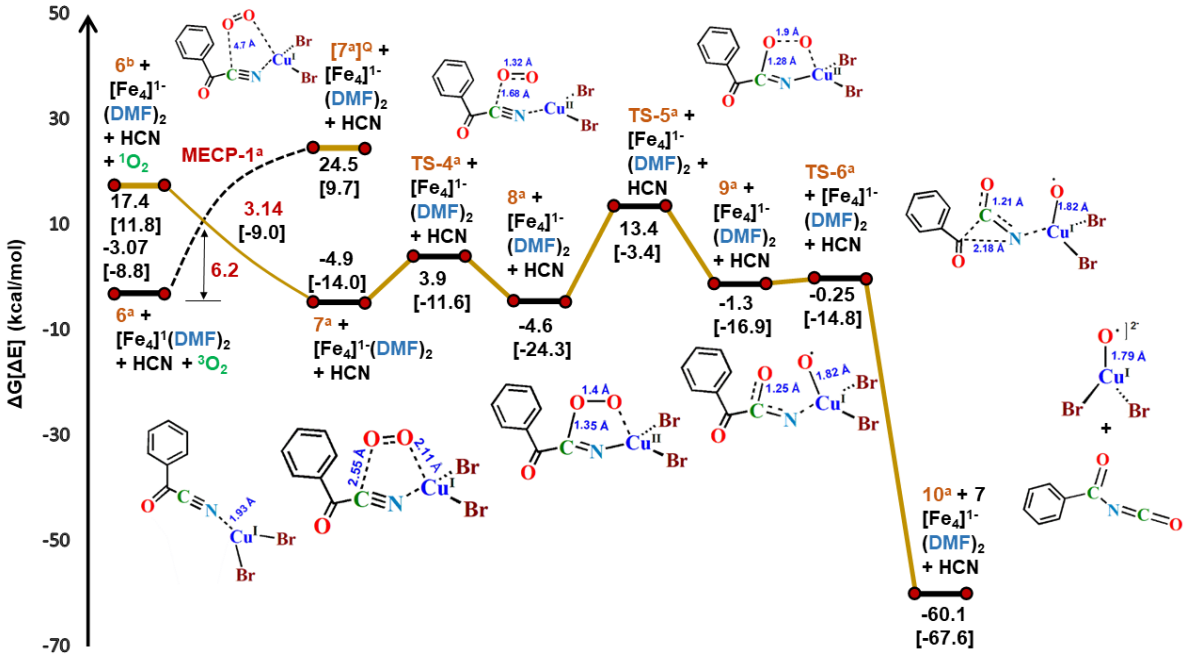

Figure 3. Computed B3LYP/B1 Gibbs free energy (ΔG) profile for activation of triplet dioxygen by $CuBr_2$-1-benzoyl cyanide intermediate, **6^a**. $[Fe(CN)_4]^{1-}$ ≡ $[Fe_4]^{1-}$ representation is used in the figure. Electronic Structure of Oxygen Incorporated Intermediates and Electron Transfer Mechanism. Quantities within the square bracket represents total energy change in kcal/mol [ΔE].

Electronic Structure of Oxygen Incorporated Intermediates and Electron Transfer Mechanism

Since the potential energy surface involves crossover of two spin states (quartet and doublet), the intermediates and transition states might be fraught with multireference character. For appropriately comprehending the correlation between electronic structure and reactivity of the oxygen incorporated intermediates along the potential energy surface, we conducted complete active space self-consistent field (CASSCF) calculations (on the DFT-optimized geometry). To consider all the orbitals involved in the oxidation reaction, an active space was constructed containing five Cu 3d based

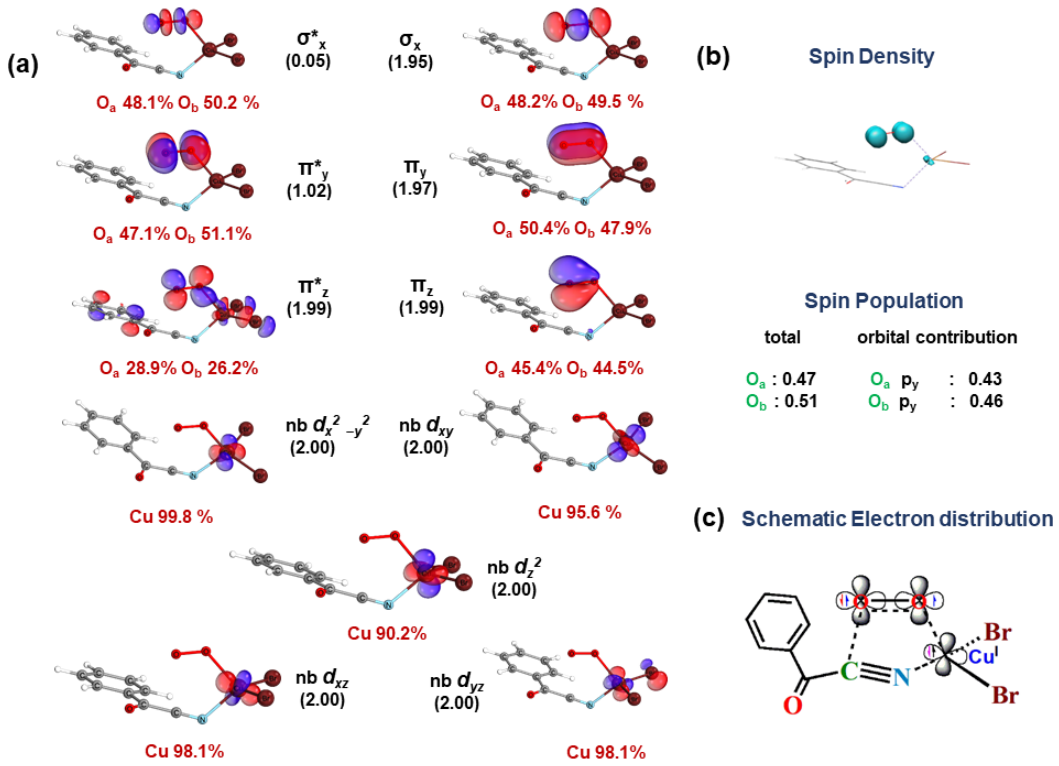

Figure 4: CASSCF (19,11) natural orbitals along with occupation numbers in parentheses for the S=1/2 state of intermediate **7[a]**. (a) Atomic contributions to each orbital are also shown. (b) Spin density, atomic spin populations and orbital contributions to the spin population (c) A schematic for electron distribution of intermediate **7[a]** is shown.

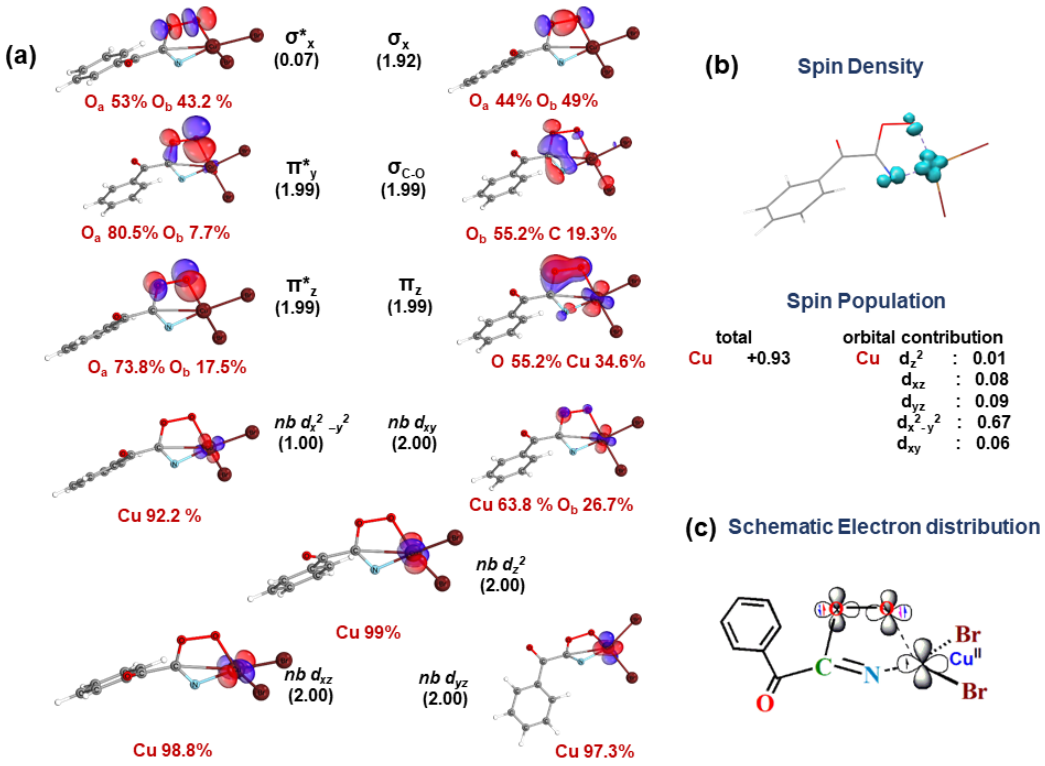

Figure 5: CASSCF (19,11) natural orbitals along with occupation numbers in parentheses for the S=1/2 state of intermediate **8[a]**. (a) Atomic contributions to each orbital are also shown. (b) Spin density, atomic spin populations and orbital contributions to the spin population (c) A schematic for electron distribution of intermediate **8[a]** is shown.

orbitals, two bonding π and antibonding π* orbitals of oxygen, and the filled σ orbitals and antibonding σ* orbital of oxygen. For all the intermediates **7[a]**, **8[a]** and **9[a]** located along the oxygen incorporation pathway, CASSCF computations were carried out using 19 electrons in 11 orbitals CAS space. CASSCF calculations revealed that the doublet ground state of complex **7[a]** contains a dominant (96 %) electronic configuration of Cu $[(d_{xy})^2(d_{x^2-y^2})^2(d_{xy})^2(d_{xz})^2(d_{z^2})^2]$ O_2 $[(\pi_{y/z})^4(\pi^*_z)^2(\pi^*_y)^1(\sigma_x)^2(\sigma^*_x)^0]$, indicating its wave function to be essentially single-reference in character. The spin density of complex **7[a]** resembles the shape of a π^*_y orbital of the oxygen moiety. This indicates the transfer of the unpaired electron residing on the carbonyl bond and nitrile moiety in complex **6[a]** to the π^*_z orbital of oxygen moiety at **MECP-1[a]**. The elongated O-O bond length (1.30 Å) confirms this electron transfer and indicates the reduction in bond order of O=O bond[34] (Figures 4 and 7). A (19, 11) CASSCF calculation was also conducted for intermediate **8[a]** with a bridging dioxygen unit for understanding its electronic structure (Figure 5). Our theoretical results predicted that the doublet ground state of **8[a]** contains a principal (96%) electronic configuration of **Cu** $[(d_{xy})^2(d_{x^2-y^2})^1(d_{xy})^2(d_{xz})^2(d_{z^2})^2]$ **O_2** $[(\pi_{y/z})^4(\pi^*_y)^2(\pi^*_z)^2(\sigma_x)^2(\sigma^*_x)^0]$ with the highest weight of the remaining electron configurations less than 5% indicating the single reference nature of its ground state wave function. The calculated spin density of complex **8[a]** resembles a shape of a d-orbital of copper and the atomic spin population analysis specifies this single occupied molecular orbital (SOMO) to be $d_{x^2-y^2}$ of Cu (Figures 5 and 7). This electronic structure analysis of complex **8[a]** indicates the transfer of an electron from the Cu^I center (d^{10} system) to the π_y^* orbital of oxygen moiety. Further elongation of O-O bond distance to 1.46 Å in **8[a]** w.r.t that of intermediate **7[a]** indicates the cleavage of the π-bond in -O-O- motif due to the filled up 2p $\pi_{y/z}^*$ orbital in intermediate **8[a]**.

Unlike the two previously discussed intermediates, a CAS(19,11) study revealed an intrinsic multireference character in **9[a]**. The CASSCF calculations indicated that the doublet ground state of intermediate **9[a]** contains two electronic structures of considerable weights, namely, **Cu** $[(d_{xy})^2(d_{xy})^2(d_{xz})^2(d_{z^2})^2]$ **Cu-N** $[(\sigma)^2$ **(**$\sigma^*)^0]$ **C=O** $[(\sigma)^2(\pi)^2]$ **O_2** $[(p_x)^1(p_x)^2(p_z)^2]$ (72%) and **Cu** $[(d_{xy})^2(d_{xy})^2(d_{xz})^2(d_{z^2})^2]$ **Cu-N** $[(\sigma)^0$ **(**$\sigma^*)^2]$ **C=O** $[(\sigma)^2(\pi)^2]$ **O_2** $[(p_x)^1(p_x)^2(p_z)^2]$ (23%) (Figure 6). Compared to the first electronic configuration, the second one indicates a two-electron excitation from the doubly occupied Cu-N σ-orbital to the unoccupied Cu-N σ*-orbital (Figure 10).

Inspection of the natural orbitals obtained from CASSCF (19, 11) calculation revealed the formation of a Cu^I-oxyl (Cu^I-$O^{\cdot}$) or Cu^{II}-oxide(Cu^{II}-O^-) moiety on one end and a carbonyl moiety on the other end at the expense of the homolytic cleavage of O-O σ bond (Figure 7). A distinguishably positive atomic spin population is noticed on the oxygen center bound to the Cu center and spin density plot of intermediate **9[a]** resembles the shape of p_x orbital of oxygen.

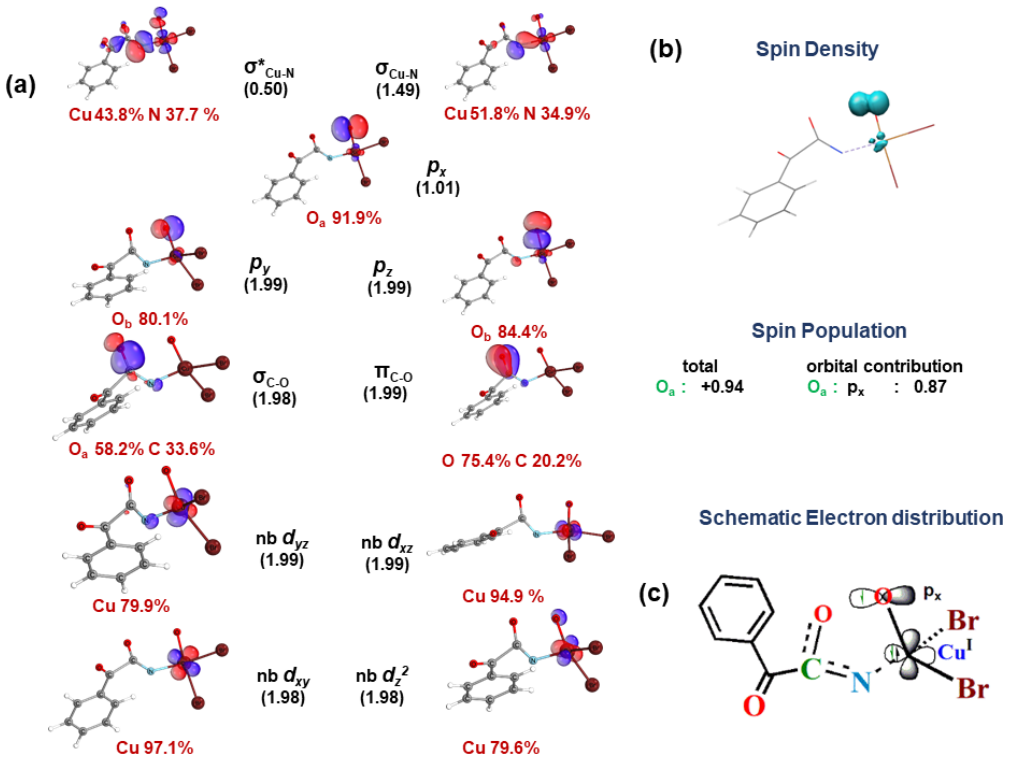

Figure 6: CASSCF (19,11) natural orbitals along with occupation numbers in parentheses for the S=1/2 state of intermediate **9[a]**. (a) Atomic contributions to each orbital are also shown. (b) Spin density, atomic spin populations and orbital contributions to the spin population (c) A schematic for electron distribution of intermediate **9[a]** is shown.

A Hoffman rearrangement [56] leads to the cleavage of Cu-N bond forming the species **10**[a], bearing the CuO moiety, the presence of which has been indicated by XPS data of the solid state samples.[20] Further, since this oxygen incorporation pathway involves many intermediates and transition states which have a radical nature, it justifies the reduction of decrease in yield of the nitrile product on addition of radical scavengers like 2,2,6,6-tetramethyl-1-piperidinyloxy (TEMPO), ascorbic acid, and 2,6-di-tert-butyl-4-methylphenol (BHT).[20]

The electronic structure analysis of intermediate **6**[a*], **7**[a*] in Pathway A* shows that a similar electron transfer mechanism as Pathway A (Figure S5 and S6 in ESI for the CASSCF natural orbital population and spin density plot for **6**[a*] and **7**[a*]) is operative.

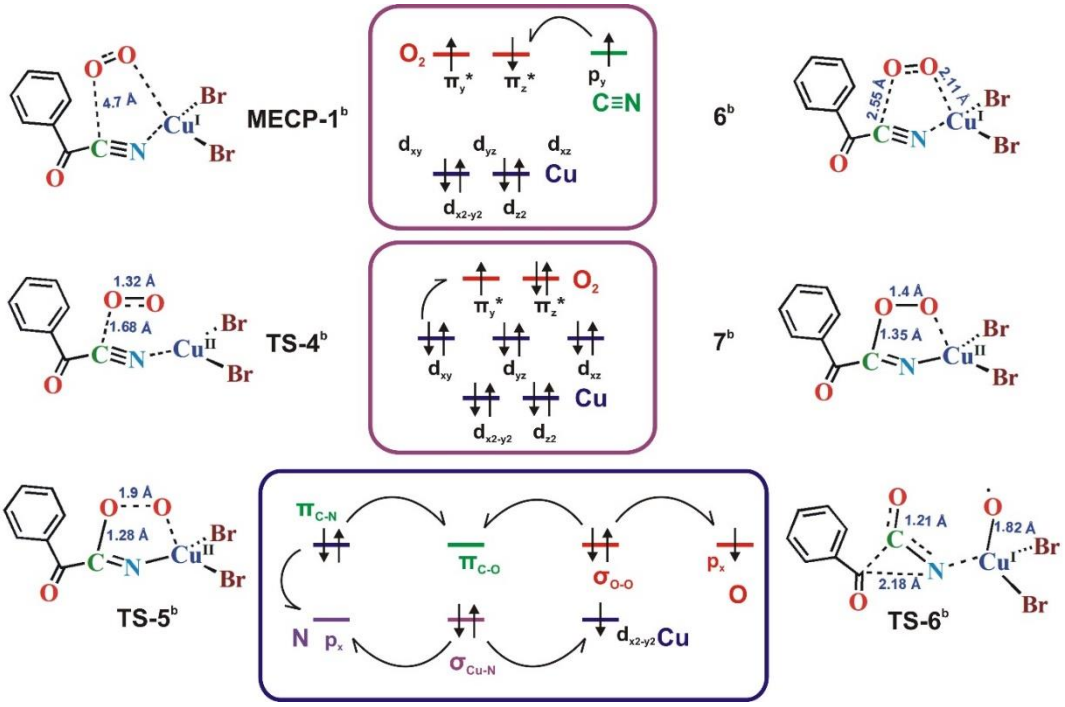

Figure 7: Schematic electron transfer pictures taking place along the oxygen incorporation PES. The highlighted box indicates the specific single electron transfer mechanism taking place between the intermediates and transition states mentioned in its left and right.

CuCN Acting Both as Copper Promoter and Cyanide Source

Similar to the Pathway A which uses Cu(II) salt for oxygen activation, we tried to find a pathway with Cu(I) salt CuCN, coordinating DMF salt with Cu(I) centre. But the hydrogen abstraction by DMF is not feasible. We carried out a scan to see the favorability of abstraction of proton by DMF solvent. The proton bound DMF solvent was found to be 37.6 kcal destabilized, hence it was deemed to be unfavorable (Figure S8 in ESI). On the other hand, You et al. have speculated that the CN bond dissociation propagates through hydrogen atom abstraction from the aldehyde leading to a radical based pathway. We investigated a prospective mechanistic corridor based on this suggestion. Molecular dynamics simulations of CuCN in DMF solvent followed by optimization of the final frame using DFT method predicted that under the experimental reaction condition Cu^{I} centre of CuCN, remains coordinated to two DMF molecules (**1**[b]) (Figure 8). In the presence of aerial oxygen at one of the coordination sites of the Cu^{I} center DMF is replaced by O_2 to form almost isoenergetic intermediate, **2**[b]. Subsequently, the Cu^{I} center is oxidized by an electron transfer to the O_2 π* orbital from the metal center and the aldehyde hydrogen atom is transferred to the oxygen center via high barrier transition state, **TS-1**[b] (37.3 kcal/mol) to form the Cu^{II}- hydroperoxide intermediate, **3**[b]. Visualization of spin density plot and analysis of spin population of intermediate,**3**[b] having triplet ground state, the two unpaired electrons were found to be residing one on the sp^2 hybridised π* orbital of C=O bond and the other on the Cu d-orbital (inset of Figure 8). Hence a benzoyl radical is formed in congruence to the proposal by Wu *et al*.[20] The π acidic character of the nitrile ligand of $Cu^{II}CN$ attracts the electron density of the Cu^{II} centre having an unpaired spin. This unpaired spin pairs up with the residual electron on the π* orbital of carbonyl bond to form a stabilised (4.3 kcal/mol) closed-shell singlet (CSS) intermediate **4**[b]. The transition state for the formation of this intermediate, **4**[b] from **3**[a] could not be located after several attempts. A σ-bond is formed between the carbon centre of the carbonyl group and the nitrogen end of the nitrile ligand attached to Cu^{II} centre of the hydro-peroxo complex in intermediate, **4**[b]. The reaction temperature being very high (415 K) and the slow reaction rate (takes 12 hours to complete) justifies the high barrier height of **TS-1**[b], in the rate determining step of

the acyl radical formation reaction pathway. The closed shell singlet intermediate **4^b** reacts with the triplet dioxygen, and via triplet transition state **TS-2^b** (29.1 kcal/mol) and minimum energy crossing point, **MECP-1^b** (29.7 kcal/mol) and leads to the formation of the singlet intermediate, **5^b** (Figure 9). Since at the MECP point the crossover of two surfaces having different spin states take place, its wavefunction is expected to have a multireference character. Hence to carefully investigate the electronic structure of **MECP-1^b**, we performed state-averaged CASSCF (18, 11) calculation (Figure S7 in ESI).

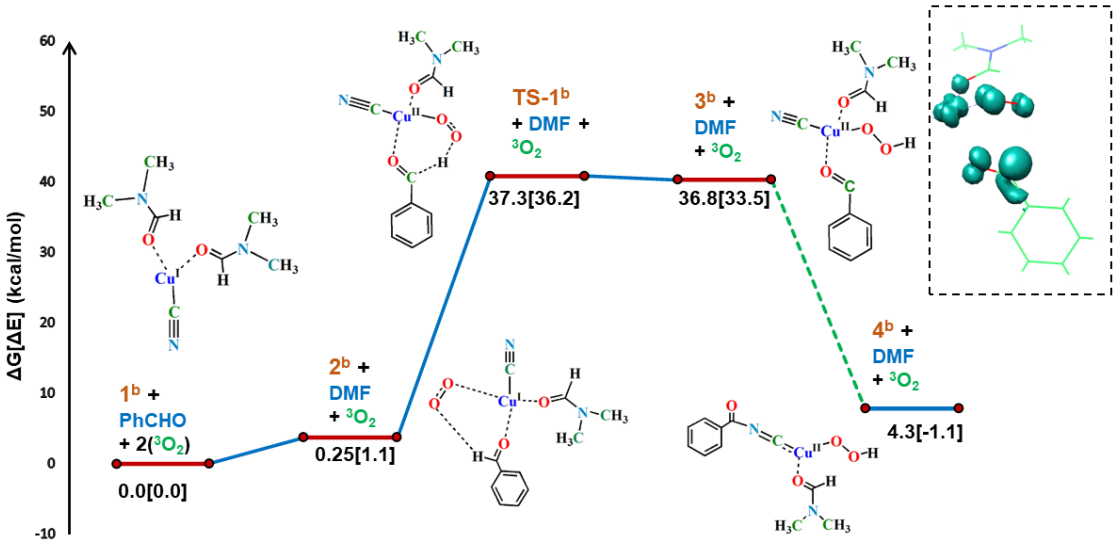

Figure 8: Computed B3LYP/B1 Gibbs free energy (ΔG) profile for benzoyl radical generation from benzaldehyde in presence of CuCN under dioxygen atmosphere (Pathway B).

The active space comprises five Cu d orbitals, two σ-bonding orbitals (Cu-O and C-O), two O_a-O_b σ and σ* orbitals, and two O_a-O_b π and π* orbital. The singlet wave function of **MECP-1^b** is found to contain two dominant configurations and hence multireference in nature. Visualization of the SA-CASSCF orbitals and analyzing the multiconfigurational wavefunction of **MECP-1^b** indicated the two unpaired electrons in the open shell singlet and the triplet state at the crossing point resides on the Cu^{II} d_{xy} orbital and the O_2 π_z* orbital. Hence an electron transfer has already occurred in the **TS-2^b** from the carbon center of the nitrile moiety to the O_2 π* orbital leading to the formation of C-O σ-bond.

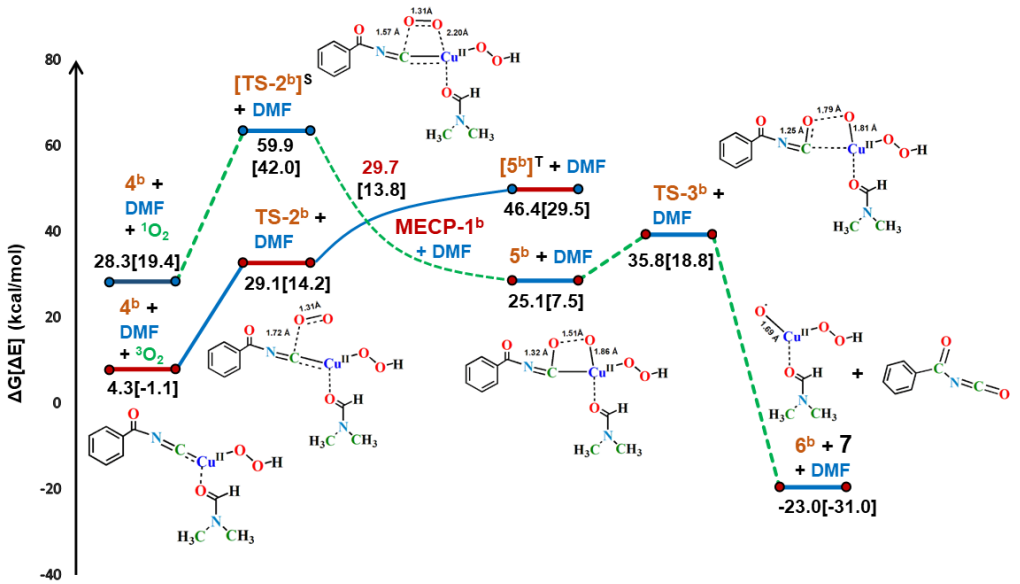

Figure 9: Computed B3LYP/B1 Gibbs free energy (ΔG) profile for oxygen activation reaction mechanism, for formation of benzoyl isocyanate from benzaldehyde in presence of CuCN under dioxygen atmosphere.

Subsequently after the spin crossover Cu-C σ bond cleaves, via **TS-3^{b}** (35.8 kcal/mol) and leads to the formation of singlet benzyl isocyanate product,**7** and an intermediate, **6^{b}** bearing Cu^{II}-$O^{\bullet}$ moiety. This copper(II)-oxyl radical moiety has been detected by XPS analysis of the solid sample of the products in the experimental work by Wu *et. al*.[20] Besides the generation of Cu^{II}-$O^{\bullet}$ (Cu^{II}-oxyl) species clearly explain the identification of an electron paramagnetic resonance(EPR) peak on addition of free-radical spin-trapping agent DMPO (5,5-dimethyl-1-pyrroline N-oxide).[20]

Computational Details

Static Quantum Computation: Geometry optimizations were carried out for all intermediates and transition states using hybrid B3LYP[35-36] density functional in combination with Pople's 6-311++G** basis for all atoms C, H, N and O except Cu. Cu was described by LANL2TZ basis set which is a combination of an effective core potential LANL2 for core electrons and a valance triple-ζ basis set for the valance electrons (B1 basis set). B3LYP functional in conjunction with empirical dispersion correction including Becke-Johnson damping (D3BJ), as implemented in Gaussian 16 was used for the first step of mechanistic pathway to check the influence of non-covalent interactions. Negligible change in the optimised structure and energetics was noticed on addition of the dispersion correction. Implicit solvent effects during optimization and single point calculation were modelled by employing polarizable continuum model (CPCM) using n,n-Dimethyl Formamide (ε=37.2) as solvent.[37] Effect of explicit solvent molecules were also checked by carrying out optimization with the solvents present in the primary solvation sphere in the guess obtained from molecular dynamics simulation. Harmonic frequency calculations were carried out at same level of theory on the optimized geometries to differentiate transition states from local minima. The local minima (intermediate) were characterized by all positive eigen values of the Hessian matrix, whereas the transition states were found to possess one negative eigen value. The entropy contribution of each solute obtained from frequency calculation is obtained through Sakur-Tetrode equation which essentially treats the molecules as ideal gas.[38] The translational entropy encounters a significant change on transition of solute molecules from gas phase to solvent phase. In order to to take into account the reduced entropy for each solute, gas phase entropy was scaled down by 50 %, following popular rigid-rotor model for estimating free energy changes in the solvent phase, as shown in previous studies.[39-41] To determine the electronic structure of several intermediates and MECP point, multireference complete active space self-consistent field (CASSCF) method was used. The B3LYP/B1 optimized geometry is used as the starting guess for state-specific CASSCF in combination with def2-TZVP triple-ζ basis set for all atoms.[42-43] To account for relativistic effects, scalar relativistic zeroth order approximation (ZORA) was used.[44-47] For the initial guess of CASSCF calculation, localized orbitals were computed according to the Pipek-Mezey scheme. On top of the CASSCF optimized orbitals, n-electron value perturbation theory (NEVPT2) calculation were carried out to include the dynamic correlation and compute the spin orbit coupling term at the MECP point. All muti-reference calculations were conducted with the ORCA 4.0.1 software package.[48]

Molecular Dynamics Computation: The classical molecular dynamics simulations of the DMF box and substrate-solvent complexes were done using the GROMACS 5.1 simulation program.[49] A cubic box of DMF molecules was built and each side of the box was 1 nm away from the centre of one of the DMF molecules. The initial topology file of DMF was taken from Automatic Topology Builder (ATB) (Molid: 9380).[50] Energy minimization with 50000 steps was carried out subsequently using the steepest descent method. The temperature was preserved at 300 K with the V-rescale algorithm[51] and the pressure was maintained by a Parrinello−Rahman barostat.[52-53] The electrostatic interactions were measured using the particle mesh Ewald summation method.[57] The long-range cut-off for non-bonded interactions was taken as 10 Å for all the above minimization steps and also for all subsequent MD simulations.[54] The whole system was then simulated for 1 ns using the NVT ensemble followed by another 1 ns simulation using NPT ensemble. The integration step for all MD simulations were 1 fs. Subsequently, 50 ns of production run simulation was performed using NPT ensemble. Monitoring of temperature, density, and trajectory analysis was performed using GROMACS 5.1 toolkit. Since the topology parameters for CuCN or $CuBr_2$ were unavailable we got the topology file for CNSe (Molid: 27365) and manually included the bonding parameters for CuCN or $CuBr_2$ into it to make respective topology files for each. The Cu-Br and Cu-CN bond lengths and force constants were calculated using Gaussian 09 using B3LYP functional and B1 basis set. Due to lack of data in atom types of the gromos54a7 force field, we had to add force field parameters (C6 and C12) for C, N atoms of cyanide moiety and bromide. Force field parameters (C6 and C12) (Table ST2 in ESI) were calculated using ε and σ values for respective atoms.[33]

Conclusion

In our present theoretical study, we have conducted an exhaustive mechanistic investigation of a copper promoted nitrogen transfer reaction to aldehyde cleaving the C≡N bond using DFT. A detailed electron structure analysis of the intermediates and transition states along with the mechanistic path using ab initio multireference CASSCF calculation has also been carried out. Our investigations have in general unraveled two distinct mechanistic channels propagating through radical intermediates as had been suggested earlier from experimental studies. Furthermore, both the

mechanistic pathways and the electronic structure analysis predict the formation of CuO species which is in accordance to the experimental findings. The mechanistic paradigms for the two promoters, CuBr2 and CuCN have inherent differences. The theoretically predicted mechanistic pathway indicates that this is a unique instance of O_2 facilitated where the O_2 activation here is initiated by single electron transfer from the carbon center of the nitrile moiety with anchorage and assistance provided by the Cu species. However, the major driving force of this nitrogen transfer reaction is the redox cycle (Cu^{II} /Cu^{I}) which act as the electron source and sink whenever necessary along the course of reaction. Hence the copper salts act as the “electron pool” in this reaction. The rate determining step(RDS) of formation of benzoyl isocyanate via the mechanistic Pathway A is 27.6 kcal/mol and Pathway B is 37.3 kcal/mol. The formation of the final product of benzyl nitrile from benzoyl isocyanate also have high barrier of RDS as predicted by previous theoretical studies.[50] These high barrier rate determining step in both the isocyanate and nitrile formation pathway may be the reason behind requirement of high reaction temperature.

.

References

[1] V. Y. Kukushkin, A. J. Pombeiro, *Chem. Rev.* **2002**, *102*, 1771-1802.
[2] F. Chen, T. Wang, N. Jiao, *Chem. Rev.* **2014**, *114*, 8613-8661.
[3] M. H. Chisholm, *Chem. Rec.* **2001**, *1*, 12-23.
[4] A. Y. Timoshkin, H. F. Schaefer, *J. Am. Chem. Soc.* **2003**, *125*, 9998-10011.
[5] G. Christian, R. Stranger, B. F. Yates, C. C. Cummins, *Dalton Trans.* **2008**, 338-344.
[6] G. Cavigliasso, G. J. Christian, R. Stranger, B. F. Yates, *Dalton Trans.* **2011**, *40*, 7327-7339.
[7] R. R. Schrock, M. L. Listemann, L. G. Sturgeoff, *J. Am. Chem. Soc.* **1982**, *104*, 4291-4293.
[8] T. Budzichowski, M. Chisholm, K. Folting, *Chem. Eur. J.* **1996**, *2*, 110-117.
[9] X. Sun, C. Wang, Z. Li, S. Zhang, Z. Xi, *J. Am. Chem. Soc.* **2004**, *126*, 7172-7173.
[10] A. M. Geyer, E. S. Wiedner, J. B. Gary, R. L. Gdula, N. C. Kuhlmann, M. J. Johnson, B. D. Dunietz, J. W. Kampf, *J. Am. Chem. Soc.* **2008**, *130*, 8984-8999.
[11] M. Bindl, R. Stade, E. K. Heilmann, A. Picot, R. Goddard, A. Fürstner, *J. Am. Chem. Soc.* **2009**, *131*, 9468-9470.
[12] J. Heppekausen, R. Stade, R. Goddard, A. Fürstner, *J. Am. Chem. Soc.* **2010**, *132*, 11045-11057.
[13] S. Zhang, J. Zhao, W.-X. Zhang, Z. Xi, *Org. Lett.* **2011**, *13*, 1626-1629.
[14] E. S. Wiedner, K. J. Gallagher, M. J. Johnson, J. W. Kampf, *Inorg. Chem.* **2011**, *50*, 5936-5945.
[15] M. Genelot, N. P. Cheval, M. Vitorino, E. Berrier, J.-M. Weibel, P. Pale, A. Mortreux, R. M. Gauvin, *Chem. Sci.* **2013**, *4*, 2680-2685.
[16] D. Coons, J. Laurie, R. Haltiwanger, M. R. DuBois, *J. Am. Chem. Soc.* **1987**, *109*, 283-285.
[17] T. Kawashima, T. Takao, H. Suzuki, *Angew. Chem. Int. Ed.* **2006**, *118*, 499-502.
[18] H. Seino, Y. Tanabe, Y. Ishii, M. Hidai, *Inorg. Chim. Acta* **1998**, *280*, 163-171.
[19] Y. Tanabe, H. Seino, Y. Ishii, M. Hidai, *J. Am. Chem. Soc.* **2000**, *122*, 1690-1699.
[20] Q. Wu, Y. Luo, A. Lei, J. You, *J. Am. Chem. Soc.* **2016**, *138*, 2885-2888.
[21] S. V. Ley, A. W. Thomas, *Angew. Chem. Int. Ed.* **2003**, *42*, 5400-5449.
[22] K. Hirano, M. Miura, *Chem. Commun.* **2012**, *48*, 10704-10714.
[23] J. Kim, J. Choi, K. Shin, S. Chang, *J. Am. Chem. Soc.* **2012**, *134*, 2528-2531.
[24] Z. Chen, Q. Yan, Z. Liu, Y. Xu, Y. Zhang, *Angew. Chem. Int. Ed.* **2013**, *52*, 13324-13328.
[25] Y. Ye, M. S. Sanford, *J. Am. Chem. Soc.* **2013**, *135*, 4648-4651.
[26] M. A. D. Aravena, F. Neese, *Inorg. Chem.* **2016**, *55*, 4457-4469.
[27] M. Nishino, K. Hirano, T. Satoh, M. Miura, *Angew. Chem. Int. Ed.* **2013**, *125*, 4553-4557.
[28] K. K. Toh, A. Biswas, Y.-F. Wang, Y. Y. Tan, S. Chiba, *J. Am. Chem. Soc.* **2014**, *136*, 6011-6020.
[29] M. Shang, S. Z. Sun, H. L. Wang, B. N. Laforteza, H. X. Dai, J. Q. Yu, *Angew. Chem. Int. Ed.* **2014**, *53*, 10439-10442.
[30] C. Zhang, C. Tang, N. Jiao, *Chem. Soc. Rev.* **2012**, *41*, 3464-3484.
[31] S. E. Allen, R. R. Walvoord, R. Padilla-Salinas, M. C. Kozlowski, *Chem. Rev.* **2013**, *113*, 6234-6458.
[32] E. A. Lewis, W. B. Tolman, *Chem. Rev.* **2004**, *104*, 1047-1076.
[33] J. N. Harvey, M. Aschi, H. Schwarz, W. Koch, *Theor. Chem. Acc.* **1998**, *99*, 95-99.
[34] C. J. Cramer, W. B. Tolman, K. H. Theopold, A. L. Rheingold, *Proc. Natl. Acad. Sci* **2003**, *100*, 3635-3640.
[35] C. Lee, W. Yang, R. Parr, *Phys. Rev. B* **1988**, *37*, 785-789.
[36] A. D. Becke, *Phys. Rev. A* **1988**, *38*, 3098.
[37] J. Tomasi, B. Mennucci, R. Cammi, *Chem. Rev.* **2005**, *105*, 2999-3094.
[38] S. Glasstone, *Thermodynamics for Chemists*, **1947**.
[39] W. X. Li H, Huang F, Lu G, Jiang J, Wang ZX., *Organometallics* **2011**, *19*, 5233-5247.
[40] Z.-X. Yu, K. Houk, *J. Am. Chem. Soc.* **2003**, *125*, 13825-13830.
[41] W. X. Li H, Wen M, Wang ZX. , *Eur. J. Inorg. Chem.* **2012**, *2012*, 5011-5020.
[42] A. Schäfer, C. Huber, R. Ahlrichs, *J. Chem. Phys.* **1994**, *100*, 5829-5835.
[43] A. R. Weigend F, *Phys. Chem. Chem. Phys.* **2005**, *7*, 3297-3305.
[44] E. V. Lenthe, Baerends, E. J., & Snijders, J. G., *J. Chem. Phys.* **1994**, *101*, 9783-9792.
[45] E. V. Lenthe, Baerends, E. J., & Snijders, J. G., *J. Chem. Phys.* **1993**, *99*, 4597-4610.

[46] E. V. Lenthe, Van Leeuwen, R., Baerends, E.J. and Snijders, J.G., *Int. J. Quant. Chem.* **1996**, *57*, 281-293.
[47] C. X. Pantazis DA, Landis CR, Neese F., *J. Chem. Theory Comput.* **2008**, *4*, 908-919.
[48] F. Neese, Max Planck Institute for Chemical Energy Conversion, Mülheim, Germany, **2017**.
[49] M. T. Abraham MJ, Schulz R, Páll S, Smith JC, Hess B, Lindahl E., *SoftwareX* **2015**, *1*.
[50] Z. L. Malde AK, Breeze M, Stroet M, Poger D, Nair PC, Oostenbrink C, Mark AE., *J. Chem. Theory Comput.* **2011**, *7*, 4026-4037.
[51] P. J. Berendsen HJ, van Gunsteren WF, DiNola AR, Haak JR., *J. Chem. Phys.* **1984**, *81*, 3684-3690.
[52] Y. D. Darden T, Pedersen L., *J. Chem. Phys.* **1993**, *98*, 10089-10092.
[53] R. A. Parrinello M, *J. Appl. Phys.* **1981**, *52*, 7182-7190.
[54] P. A. A. Canongia Lopes J. N., *J. Phys. Chem. B* **2006**, *110*, 19586-19592.
[55] P. D. W. Boyd, M. G. Glenny, C. E. F.Rickard, A. J. Nielson, Polyhedron **2011**, *30*, *632*
[56] W. Everett, J. Lane, *The Hofmann Reaction*. *Organic Reactions*. **1946**, *3*, *267–306.*
[57] T. Darden, D. York, L. Pedersen, *J. Chem. Phys.* **1993**, *98*(12), 10089-10092.

Table of Content